Polymer Testing 136 (2024) 108487

Contents lists available at ScienceDirect

Polymer Testing

journal homepage: www.elsevier.com/locate/polytest

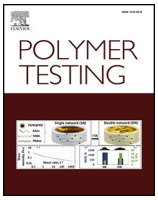

Contribution of the radiative transfer mechanism to the total thermal conductivity of anisotropic porous materials

Jorge Torre [a,b,c,*], Victoria Bernardo [d], Javier Pinto [a,b,c], Miguel Ángel Rodríguez-Pérez [a,b]

[a] Porous Materials Laboratory (CellMat), Condensed Matter Physics, Crystallography, and Mineralogy Department, Faculty of Science, University of Valladolid, Spain
[b] BioEcoUVA Research Institute on Bioeconomy, University of Valladolid, Spain
[c] Study, Preservation, and Recovery of Archaeological, Historical and Environmental Heritage (AHMAT) Research Group, Condensed Matter Physics, Crystallography, and Mineralogy Department, Faculty of Science, University of Valladolid, Spain
[d] CellMat Technologies S.L., Edificio PC-UVA, Paseo de Belén 9A, 47011, Valladolid, Spain

ARTICLE INFO

Keywords:
Thermal insulation
Extrusion
Polymers
Anisotropy
Infrared radiation

ABSTRACT

In order to understand the performance of polymeric porous materials as heat insulators, the contribution of the radiative transfer mechanism in porous materials with high ratios of anisotropy is studied. Porous materials based on extruded polystyrene (XPS) with relative density in the range of 0.03 – 0.05 and with a range of anisotropy ratios of 0.6 – 1.4 have been selected for this research. The study begins with a characterization of the selected materials in terms of porous structure and thermal conductivity as a function of temperature. Then, the radiative contribution for each of the three main directions of the materials is obtained by three independent methodologies: Fourier Transform Infrared (FTIR) spectroscopy, derivation from the total conductivity using theoretical models, and theoretical calculation from the model proposed by Glicksman. The results show similar trends for all methods and confirm clear differences between each direction, showing a significant reduction of the radiative contribution and, thus, the total conductivity, if the material is oriented geometrically towards the direction in which the pore size is the smallest. Indeed, reductions of 17 – 20% in the total conductivity can be achieved at temperatures ranging from 10 – 40 $^{\circ}C$ if the material is reoriented as stated.

1. Introduction

Households are responsible for a significant share of the global energy consumption. Indeed, the building sector is the second most consuming sector in the European Union (EU) (27%), only surpassed by transportation (31 %) [1]. One of the most acknowledged means of reducing the amount of energy used in households is by enhancing its efficiency with the use of improved thermal insulators [2,3].

Polymeric porous materials are well known for their capability to present low thermal conductivities, low density, low cost, and ease of production and installation [4]. Some of the most common porous materials used nowadays for insulation purposes are extruded polystyrene (XPS), expanded polystyrene (EPS), and rigid polyurethane foams (RPU) [5]. Hence, understanding and improving their performance as heat insulators is beneficial from both environmental and economical points of view.

Among the diverse types of polymeric porous materials, closed pore exhibit the lowest thermal conductivity. This is due to their minimal volume fraction of the solid phase and the low conductivity of the gas encapsulated within the pores [6,7]. Additionally, when the pore size is lower than 4 *mm*, convection is negligible (see section 2). A common way authors have approached the problem of understanding the thermal conductivity is taking into account the four mechanisms of heat transfer: conduction through the solid phase, conduction through the gas phase, convection, and radiation [8–13]. In low density porous materials, this last term can reach up to 40% of the total thermal conductivity [14–16]. That is the main reason why several authors have previously studied this topic. Some of them focused on the theoretical prediction of the radiative heat transfer of different types of polymeric porous materials. For instance, Glicksman et al. [17] reviewed different approaches for the theoretical study of the radiative term, evaluating their reliability comparing their results with experimental values obtained for polyurethane foams. Williams and Aldao [18] derived a theoretical equation without adjustable parameters considering unidirectional heat flow through an ideal foam with equally separated semi-transparent

* Corresponding author. Porous Materials Laboratory (CellMat), Condensed Matter Physics, Crystallography, and Mineralogy Department, Faculty of Science, University of Valladolid, Spain.
E-mail address: jorge.torre@uva.es (J. Torre).

https://doi.org/10.1016/j.polymertesting.2024.108487
Received 8 April 2024; Received in revised form 22 May 2024; Accepted 12 June 2024
Available online 13 June 2024

Nomenclature

$E_{b,\lambda}$	black body spectral emissive power
E_b	black body total emissive power
f_s	fraction of mass in the struts
g	geometrical factor
K_R	Rosseland extinction coefficient
K_G	Glicksman extinction coefficient
K_w	solid polymer extinction coefficient
K_λ	spectral extinction coefficient
L	sample thickness
m	linear regression slope
n	real refractive index
R	anisotropy ratio
T	temperature
T_λ	transmittance
φ	mean pore size
Φ	energy flux
λ	wavelength
$\overline{\lambda}_c$	convection tensor
$\overline{\lambda}_g$	gas conduction tensor
$\overline{\lambda}_r$	radiative transfer tensor
$\overline{\lambda}_s$	solid conduction tensor
$\overline{\lambda}_T$	total conductivity tensor
λ_c	convection contribution
λ_g	gas conduction contribution
λ_r	radiative transfer contribution
λ_s	solid conduction contribution
λ_T	total thermal conductivity
λ_{air}	air thermal conductivity
λ_{solid}	solid polymer thermal conductivity
ρ_r	relative density
σ	Stephan-Boltzmann constant

Superscripts

i	i direction

membranes, disregarding struts. Kuhn et al. [19] obtained the spectral specific extinction coefficient and, thus, the radiative term, using Mie scattering theoretical calculations for polystyrene foams. Other authors such as Heinemann and Caps [20], Tseng and Kuo [21] or, more recently Arduini et al. [11], showed an experimental approach to measure the extinction coefficient, a key parameter in the radiative contribution, for polyimide, phenolic, and polystyrene and polyurethane foams respectively. They achieved it by performing measurements with FTIR spectroscopy and applying the diffusion approximation, i.e. using the Rosseland equation, which will be discussed in the theoretical background section in this work.

Most porous polymers are anisotropic as a consequence of the production process (see Supplementary Information, Figs. 1 and 2) [22]. Extrusion foaming is a very common process used nowadays to produce commercial foams, such as polystyrene foams, polyethylene foams, polypropylene foams, polylactic acid foams, polyetherimide foams etc [5,23]. In the case of extrusion foaming, it is common to produce porous structures with a clear directionality. In fact, extrusion foaming is a directional process in which three axes are usually defined. These are the machine direction (MD), the transverse direction (TD) and the thickness direction (Z) [5]. Therefore, materials can be characterized by a certain degree of anisotropy associated with different pore sizes in three orthogonal directions. Anisotropy has been found to have impact on the total thermal conductivity of porous materials [24]. One of the reasons is that anisotropy is expected to have an influence on the radiative heat transfer mechanism, making it behave differently in each direction.

Despite the numerous works in the literature about the analysis of the radiative contribution, and those about the effect of anisotropy in the total thermal conductivity, none has been found in which the effect of the anisotropy of the porous structure in the radiative contribution is studied in detail. Hence, this research work aims to cover this gap analysing the radiation contribution in three orthogonal directions for different extruded polystyrene foams with a variety of ratios of anisotropy using different methods.

2. Theoretical background

Fourier's law of heat transfer states that the energy flux Φ (i.e., heat energy per unit time and cross-sectional area) passing through a homogeneous volume is proportional to, and in the direction of, the negative temperature gradient between both sides (see Equation (1)):

$$\Phi = -\overline{\lambda}_T \nabla T, \tag{1}$$

being $\overline{\lambda}_T$ the proportionality second-order tensor for anisotropic materials. The homogeneity assumption is a good approximation as long as the pore size is sufficiently small compared to the external dimensions of the materials [16]. Given that porous materials can be considered as orthotropic materials – this is, they present symmetry under orthogonal transformations – , in the correct orthogonal basis, λ_T can be written as [25,26]:

$$\overline{\lambda}_T = \begin{pmatrix} \lambda_T^{xx} & 0 & 0 \\ 0 & \lambda_T^{yy} & 0 \\ 0 & 0 & \lambda_T^{zz} \end{pmatrix}, \tag{2}$$

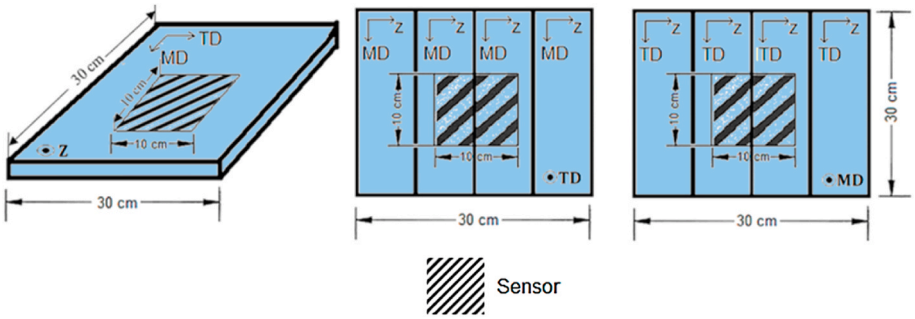

Fig. 1. Dimensions and disposal of the samples and heat flow sensor used for measuring the thermal conductivity in different directions of the samples from Table 1.

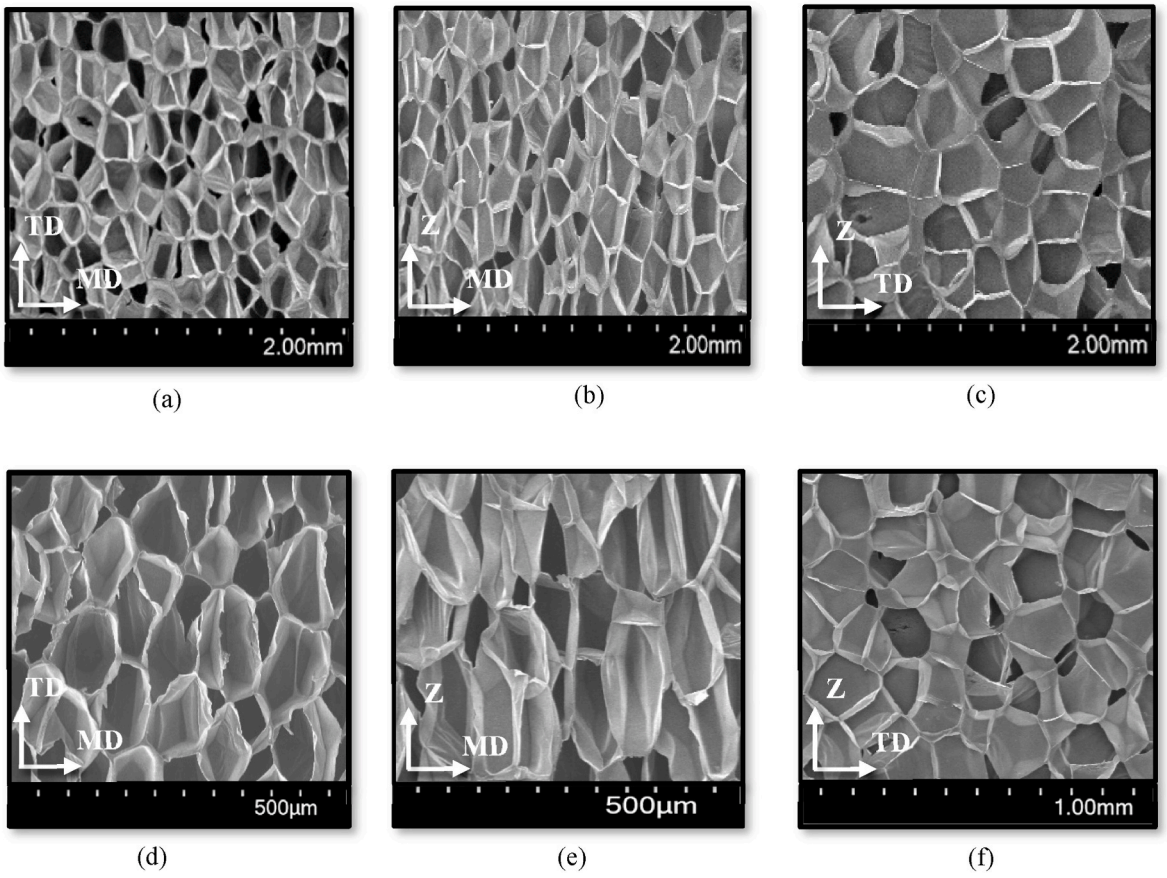

Fig. 2. SEM micrographs of the three orthogonal cross-sectional areas of BXPS1 (a–c) and BXPS2 (d–f).

where each $\lambda_T^{ii}, i = x, y, z$, is the total thermal conductivity in the i direction. In porous materials produced by extrusion foaming, it is common to use the orthogonal directions MD, TD and Z, where MD represents the machine direction of the extrusion process, TD the transverse one, and Z the perpendicular to both [27], as shown in Supplementary Information, Fig. 2.

In the case of polymeric porous materials, the heat transfer process can be broken down into four contributions as shown in Equation (3): conduction through the solid phase λ_s, conduction through the gaseous phase λ_g, radiation transmission λ_r, and heat convection λ_c [8–13]. This is typically an accurate approximation which considers independence between all heat transfer mechanisms [6,8].

$$\bar{\lambda}_T = \bar{\lambda}_s + \bar{\lambda}_g + \bar{\lambda}_r + \bar{\lambda}_c \tag{3}$$

While the convection term can be neglected for porous materials with pore sizes under 4 *mm*, and in fact, it will be neglected here, the other ones cannot [5,8,28]

Considering from now on the conductivities in only one direction and removing the superscript for the sake of notational simplicity, each term in Equation (3) can be theoretically modelled as follows [5,8,16]:

2.1. Conduction through the solid phase λ_s

This contribution accounts for about 10 – 15% of the total conductivity in typical XPS foams [3]. The solid polymer in a porous material takes the form of pore walls and struts as can be seen in the Supplementary Information, Fig. 3a). Therefore, heat moves in non-linear paths. An approximated model proposed by Glicksman can be used to predict the contribution of conduction through the solid as shown in Equation (4). The model considers that the solid contribution can be calculated as the thermal conductivity of the solid polymer multiplied by the volume fraction of solid or relative density (ρ_r) in the material and a geometrical correction factor.

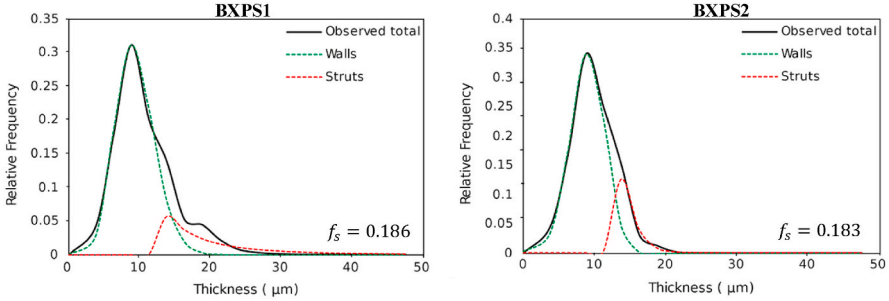

Fig. 3. Observed total thicknesses distribution of walls and struts for the materials from Table 1. The dotted lines represent the deconvoluted peaks of distribution of walls and struts separately.

$$\lambda_s^i = g\rho_r\lambda_{solid} = \left(\frac{1}{3}f_s\sqrt{R^i} + \frac{2}{3}(1-f_s)\sqrt[4]{R^i}\right)\rho_r\lambda_{solid}, \quad (4)$$

In Equation (4), g is the geometrical factor of the material, which can be expressed in terms of the fraction of mass in the struts f_s and the anisotropy ratio in the i direction R^i (more details can be found in the Supplementary Information, S2). Therefore, this model accounts for structural parameters such as the shape of the pores or the pore wall thickness [8]. Also, in Equation (4), ρ_r is the relative density of the foam, obtained as the ratio between the density of the foam and the one of the solid material, and λ_{solid} is the total conductivity of the solid polymer.

2.2. Conduction through the gas phase λ_g

This mechanism is the most contributing one, typically accounting for about 60 to 70% of the total conductivity for microporous polymers [3]. The case of nanoporous polymers is different, as the Knudsen effect starts playing an important role in decreasing the conduction through the gas phase (see Ref. [29]). However, as microporous polymers are considered in this work, the conduction through the gas phase can be simply modelled by multiplying the conductivity of the gas, which is air for the foams under study (λ_{air}), by the volume fraction of air (or porosity) of the foam, which is related with the relative density [30]:

$$\lambda_g = \lambda_{air}\frac{(3/2-\rho_r)}{3/2-\rho_r/2} \quad (5)$$

2.3. Radiative transfer λ_r

This term can be responsible for about 10 to 40% of the total conductivity [3,4,15]. For samples with enough thickness, the radiation process can be regarded as a diffusion process (diffusion approximation). Under the hypothesis that the scattering is isotropic and the radiation mean free path is much shorter than the foam thickness, the Rosseland equation states that the radiative contribution can be written as [8]:

$$\lambda_r = \frac{16n^2\sigma T^3}{3K_R}, \quad (6)$$

where σ is the Stefan-Boltzmann constant, T is the material temperature, n is its refractive index (approximately 1 for low density porous materials [7]) and K_R is the Rosseland extinction coefficient obtained experimentally as shown in subsection 3.2.3. As it can be seen from Equation (6), the Rosseland extinction coefficient is an essential parameter for the calculation of the radiative transfer contribution.

Glicksman et al. [8] proposed a theoretical method to compute this extinction coefficient K_R for polyurethane closed-pore foams. They considered an isotropic porous media with regular pentagonal dodecahedral cells, which is very close to reality in many different foams [16], and randomly oriented blackbody struts. For the struts' contribution, they considered that its cross-sectional area was constant and it occupied two-thirds of the area of an equilateral triangle. For the walls contribution, they assumed thin enough pore walls to be able to approximate the radiation directional transmissivity by its Taylor series to the first order (optically thin limit). The expression for the extinction coefficient proposed by these scientists (K_G) can be seen in Equation (7):

$$K_G = K_{edges} + K_H K_w = 4.10\frac{\sqrt{f_s\rho_r}}{\varphi} + (1-f_s)\rho_r K_w, \quad (7)$$

where φ is the mean pore size of the porous polymer and K_w is the extinction coefficient of the solid polymer.

3. Experimental procedure

3.1. Materials

The set of polymeric porous materials that was selected for this study is composed of two commercial extruded polystyrene (XPS) foams of big dimensions ($30 \times 30 \times 7.5$ *cm*) and high anisotropy ratios, which were kindly provided by Isofoam (Kuwait). The samples were produced by an extrusion process (see Supplementary Information, Fig. 2) of amorphous polystyrene, using CO_2 and *EtOH* as physical blowing agent agents, talc as nucleation agent, and a polymeric flame retardant based on bromine. A few weeks after production, it is known that the gases used as blowing agents diffuse out of the foam and air diffuses into the pores [3]. As our study was conducted six months after the foams production, it is possible to consider that air is inside the pores of all the porous polymers under study.

3.2. Material characterization

3.2.1. Density

In order to obtain the relative density ρ_r, the density of the solid polymer, ρ_s was considered to be 1050 kg/m^3 [15,29]. The foams density was measured using the geometrical method for the entire $30 \times 30 \times 7.5$ *cm* samples. This method consists in accurately measuring the volume and the mass of the material using a calliper and a precision balance respectively, and performing their quotient. The results are shown in Table 1. The standard deviation of this measurement was 1.5%.

3.2.2. Porous structure parameters

The pore size was measured using the software AutoCell. This tool uses images from an optical microscope *Jiusion 40A x1000*. First, the samples were prepared cutting a 1*x*1 *cm* piece and softly painting its surface with black paint so the pore walls were detectable by AutoCell [31]. Then, for each direction, three micrographs were taken in different spots of the foam and introduced in the software, which automatically computed the mentioned foam parameters. The standard deviation of the pore size measurements, calculated considering the whole population of pore sizes, was 4 %. After this, the anisotropy ratio was computed following the method exposed in the Supplementary Information, S2, Equation (1). Error propagation yielded a standard deviation of 5% for anisotropy ratios. The overall porous structure was also evaluated using *Scanning Electron Microscopy* (SEM) with a FlexSEM 1000, Hitachi model.

The fraction of mass in the struts f_s, was measured using X-ray tomography with the methodology developed by S. Pérez-Tamarit et al. [32]. The experimental set-up consisted of a micro-focus cone-beam X-ray source L10101 from Hamamatsu (spot size: 5 μm, Voltage: 20–100 kV, Current: 0–200 μA) with a maximum output power of 20 W and a flat panel detector C7940DK-02 also from Hamamatsu (2240 $\times$ 2344 pixels^2, 50 μm of pixel size). For the data treatment, ImageJ/Fiji [33] was used to obtain the information of the solid phase and Peakfit [34] for distinguishing between the pore walls and the struts information. For a more accurate explanation of this method of characterization, see Supplementary information, S3.

3.2.3. Radiative contribution λ_r

For the samples from Table 1, the parameter λ_r was obtained using

Table 1
Name of the selected samples and calculated relative density.

Sample name	Relative density ρ_r
BXPS1	0.033
BXPS2	0.046

three different methodologies, which are described below:

I) FTIR spectroscopy method.

In order to obtain the Rosseland extinction coefficient K_R in Equation (6), transmittance measurements were carried out. For this, several samples of thicknesses in the range of $0.8 - 6.3\ cm$ were cut for the three principal directions for each foam in Table 1. The samples thickness (L), was precisely measured using a DMA7 device from PerkinElmer. After that, the samples were subjected to transmission FTIR spectroscopy in a Bruker Tensor 27 with a LN-MCT Mid 2×2mm detector. The experiment was conducted in the interval of wavenumbers from 4000 to 600 cm^{-1} with a resolution of $2\ cm^{-1}$. Hence, a total of 3562 data points were collected. This interval of wavenumbers is of high relevance as the structural information on the target matter is mostly readily available from its mid-infrared spectrum [35]. In addition, the values of the number of scans, the aperture setting, the phase resolution and the correction noise were 32, 6 *mm*, 8 and 25 points respectively.

Once the transmittance was obtained, a methodology similar to the one proposed by R. A. Campo et al. [7] was used to compute K_R. According to Beer's law, the spectral extinction coefficient K_λ for homogeneous samples in which radiation extinction remains constant along the thickness can be obtained as it follows [36]:

$$T_\lambda = \exp\left(- \int_0^L K_\lambda \, dx \right) \rightarrow K_\lambda = -\frac{\ln(T_\lambda)}{L}, \tag{8}$$

where T_λ is the transmittance and L is the sample's thickness. Therefore, the spectral extinction coefficient can be obtained with a linear regression of the dependency of $\ln(T_\lambda)$ with L.

Once K_λ is obtained, the Rosseland extinction coefficient can be computed as follows [36,37]:

$$\frac{1}{K_R} = \frac{\int_0^\infty \frac{1}{K_\lambda} \frac{\partial E_{b,\lambda}}{\partial T} d\lambda}{\int_0^\infty \frac{\partial E_{b,\lambda}}{\partial T} d\lambda} = \int_0^\infty \frac{1}{K_\lambda} \frac{\partial E_{b,\lambda}}{\partial E_b} d\lambda, \tag{9}$$

where $E_{b,\lambda}$ is the black body hemispherical emissive power and E_b is the black body total emissive power. This integral was solved analytically for the purposes of this work. A standard deviation of 10% was estimated for the values of K_R obtained.

II) Method of subtraction of contributions from the total conductivity.

The radiative contribution λ_r can be obtained by means of subtracting the λ_s and λ_g terms from the total conductivity in Equation (3). For this, the total conductivity λ_T was measured on the samples in Table 1 using a steady heat flow conductivity meter Laser Comp FOX314 (Waters Corporation, USA) in agreement with the ASTM C518 method [38]. This conductivity meter was provided with a $10 \times 10\ cm$ sensor in a $30 \times 30\ cm$ cavity. Therefore, the samples could fit in, covering the whole sensor. In order to measure the total conductivity in the three main directions, a specific arrangement of the samples was used (Fig. 1). For the study of each of the directions MD and TD, four pieces of the main material sheet were cut, rotated, and put together next to each other. The chosen mean temperatures between the plates were $10, 20, 25, 30$ and $40\ ^\circ C$. This was done setting a difference in the temperature of each plate of ΔT of $20^\circ C$. The standard deviation of this measurements was 2%.

III) Glicksman's model method.

For this last method, Equation (7) was used to calculate the Rosseland extinction coefficient with the experimental values of f_s, ρ_r, and φ in each direction. Regarding K_w, it was considered to be the Rosseland extinction coefficient of the solid polystyrene, which was obtained with the FTIR spectroscopy method for a thin polystyrene (PS) film leading to a value of $43.1 \pm 4.3\ cm^{-1}$.

4. Results and discussion

4.1. Structural characterization

In order to carry out a study on the effects of anisotropy, focus has to be given to parameters such as pore size and anisotropy ratio. The results of these two variables are shown in Table 2. As it can be seen, the selected foams have considerable anisotropy ratios. A visual example of this is Fig. 2b), where the anisotropy is clearly observable, given that the majority of pores are oriented towards the Z direction in the MD-Z plane.

The pores follow the same trend in both materials: $\varphi^Z > \varphi^{TD} > \varphi^{MD}$, being the difference between the mean pore size in Z and MD very large. The anisotropy ratio in the Z direction reaches a very high value of 1.38 for the sample BXPS1 and 1.34 for the sample BXPS2. Conversely, the anisotropy in the MD direction reaches a low value of 0.66 for the sample BXPS1 and 0.63 for the sample BXPS2. The results show that the pores are clearly larger in the sample with lower density (BXPS1).

In addition, the results of the fraction of mass in the struts f_s for both materials are shown in Fig. 3, where the total observed distribution of thicknesses of walls and struts is seen, as well as the deconvolution of each one. Although the porous structure and the density of these two materials are different, the distribution of mass in struts and walls is similar. This is the expected result for XPS foams, in which the mass is mainly concentrated in the walls, and, therefore, the values of f_s are typically below 0.2 [3].

The fraction of material in the struts for both materials is close to 0.18, which means that around 82% of the mass is located in the pore walls and only 18% of the mass is located in the struts.

4.2. Thermal conductivity characterization

The results of the total conductivities in the three directions MD, TD and Z are given in Fig. 4. For both materials and all directions, the thermal conductivity increases with temperature. It can be observed that there are noticeable differences in the total conductivities between the three main directions. In fact, changing the orientation from Z to TD can account for about $3 - 4\ mW/(m \cdot K)$ in the BXPS1 foam and about $2.5 - 4\ mW/(m \cdot K)$ in the BXPS2 foam, while changing from the Z to the MD direction, can do it for about $7 - 10\ mW/(m \cdot K)$ in the BXPS1 foam and about $6 - 8\ mW/(m \cdot K)$ in the BXPS2 foam. These differences mainly come from the radiative contribution, as the solid one is very low, as proved further, and the gas conduction does not depend on pore size [16], something that will also be proved further in this work. Also, it is interesting to see that the total conductivity of the BXPS2 sample is, for each individual temperature and direction, lower than that of BXPS1. This is due to its higher relative density and lower pore size, which diminish the contributions of the two most influential mechanisms (as will be proven in the results of this work): radiative transfer and conduction through the gas. Differences between both materials can also be seen in the slope of lines in all directions. The slopes for BXPS1 are greater than those of BXPS2. Considering the previous theoretical approximations, this is due to radiative term, and, specifically, to the diverse foam parameters that affect the parameter K_R accompanying T. For example, lower relative density would imply lower K_R, and, therefore, greater slope.

Table 2
Results of the main porous structural parameters for the materials from Table 1.

Sample	$\varphi^Z(\mu m)$	$\varphi^{TD}(\mu m)$	$\varphi^{MD}(\mu m)$	R^Z	R^{TD}	R^{MD}
BXPS1	348	292	212	1.38	1.04	0.66
BXPS2	197	177	117	1.34	1.12	0.63

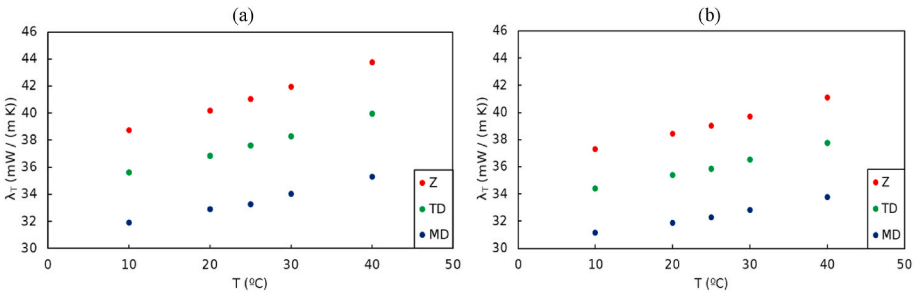

Fig. 4. Dependence of the total conductivity of the (a) BXPS1 and (b) BXPS2 as a function of temperature.

4.3. Extinction coefficient

The results of the Rosseland extinction coefficient obtained by the three methodologies outlined in section 3.2 are shown here.

I) FTIR spectroscopy method.

Fig. 5 shows an example of spectra obtained for the various thicknesses of the BXPS1 sample in the Z direction. Using a linear regression with Equation (8), an array of K_λ arises as in the example of Fig. 6. As it can be seen from Fig. 6, there are nonzero extinction coefficients outside the absorbing bands. These are due to the Mie scattering phenomena in the walls and struts' boundaries, which grow in number as the sample thickness increases.

The values of the Rosseland extinction coefficient in different directions obtained by the FTIR spectroscopy method are listed in Table 5. As it can be directly seen, there are clear differences in the extinction coefficient between directions due to the anisotropic character of the pore size. The tendency $K^{MD} > K^{TD} > K^{Z}$ is observed in both materials and this is directly related to the fact that $\varphi^{Z} > \varphi^{TD} > \varphi^{MD}$. In those directions in which the pore size is larger, the radiation finds less pore walls and struts in its path per unit length and, therefore, has a larger mean free path. It is worth to mention that, despite the fact that some peaks are saturated at some sample thicknesses, the error obtained integrating over the whole spectrum without considering the missing contribution of each saturated peak is negligible to the purposes of this work.

A separation between the scattering and the absorption contribution to K_R was also possible by means of a base line fitting. The base line of each spectrum was calculated assigning the same constant value of transmittance to every wavenumber, making sure it describes the non-absorbing regions as optimally as possible. The results of these two contributions are in accordance with the expected: the absorption contribution has a decreasing dependence with the increase in pore size because of the lower number of pores per unit length, whereas the scattering contribution has a much larger dependence with pore size because of the lower number of scattering points as the number of pores per unit length decreases. In fact, the reduction of the radiative contribution essentially comes down to this phenomenon. In the interphases between the air and the polymer, the refractive index takes complex values, leading to random scattering. Therefore, the higher the number of interphases, the higher the amount of scattered radiation outwards. This is clearly visible in Table 3.

It is also observable that the absorption contribution in the BXPS2 material is significantly larger than in BXPS1. This is directly related to the fact that the BXPS2 material density is higher with respect to the other: if there are more polymer molecules per unit length in one material with respect to the other, more absorption takes place.

A study on how much does K_R increase when the pore size reduces can be carried out by means of a linear regression of the ratios between those magnitudes. It is found that the ratio between extinction coefficients follows a linear relation with the reciprocal of pore size:

$$\frac{K_R^i}{K_R^j} = A\frac{\varphi^j}{\varphi^i} + B, A = 0.5, B = 0.6 \tag{10}$$

Interestingly, this means that reorienting the material towards a direction with half the pore size will increase K_R an amount of 1.6 times the previous value. In this case, the coefficient of determination (R^2) was 0.80 (see fit graph in section 4.4). Here, even though R^2 may not approach 1, this does not affect choice of linear fit. That value of R^2 is due to inherent variability in the measurement, as can be seen by the oscillations of points around the linear, or any given standard fit.

II) Method of subtraction of contributions from the total conductivity.

The results of the Rosseland extinction coefficient yielded by this method are shown in Table 4. Again, a similar tendency to the one obtained by the FTIR spectroscopy is found, i.e. $K^{MD} > K^{TD} > K^{Z}$. For this particular case, the numerical results for both materials are closer, so the effect of the different density and pore size is not clearly detected using this approach.

In this case, a quadratic relation is found between the ratio of

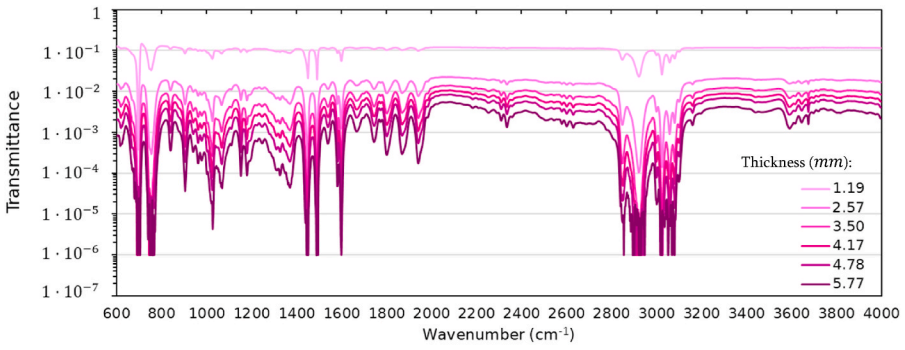

Fig. 5. Transmittance spectra of several BXPS1 samples of different thicknesses with the infrared radiation passing in the *Z* direction.

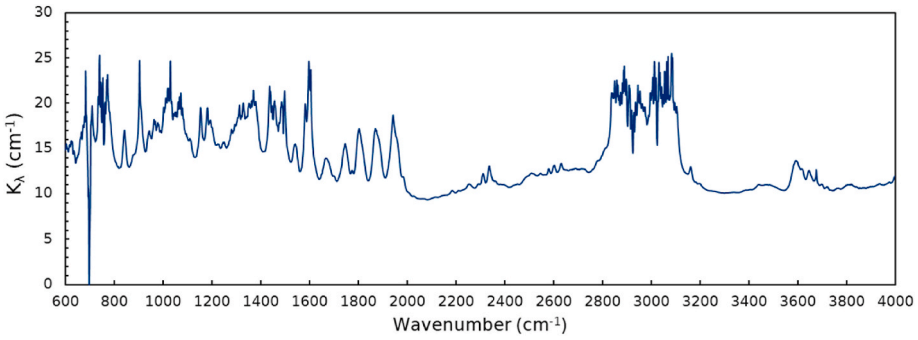

Fig. 6. Spectral extinction coefficient K_λ for a BXPS1 set of samples when the infrared radiation is passing in the Z direction.

Table 3
Results of K_R for the materials from Table 1 obtained using the FTIR method.

FTIR Spectroscopy					
Sample	Direction	φ (μm)	K_R (cm^{-1})		
			Total	Scattering	Absorption
BXPS1	MD	212	19.8	13.5	6.3
	TD	292	15.4	9.49	5.9
	Z	348	13.8	8.35	5.4
BXPS2	MD	117	20.2	11.1	9.1
	TD	177	16.6	7.68	8.9
	Z	197	14.7	5.82	8.8

Table 4
Results of K_R for the materials from Table 1 obtained using the subtraction method.

Subtraction method			
Sample	Direction	φ (μm)	K_R (cm^{-1})
BXPS1	MD	212	18.9
	TD	292	11.8
	Z	348	8.3
BXPS2	MD	117	20.8
	TD	177	11.6
	Z	197	8.10

Table 5
Results of K_R for the materials from Table 1 obtained using the Glicksman's method.

Glicksman's method			
Sample	Direction	φ (μm)	K_R (cm^{-1})
BXPS1	MD	212	16.3
	TD	292	12.2
	Z	348	10.5
BXPS2	MD	117	34.0
	TD	177	23.1
	Z	197	20.9

extinction coefficients and pore sizes. Indeed, this relation can be obtained if a quadratic regression is performed:

$$\frac{K_R^i}{K_R^j} = A\left(\frac{\varphi^j}{\varphi^i}\right)^2 + B\frac{\varphi^j}{\varphi^i} + C \rightarrow \quad A = 4.9, B = 12.0, C = 8.7 \tag{11}$$

Here, a coefficient of determination (R^2) of 0.99 was obtained.

III) Glicksman's model method.

In this section, the results obtained applying the theoretical model proposed by Glicksman are studied. Table 5 shows the Rosseland extinction coefficient calculated by this method. Again, the same tendency is observed: the lower the pore size in any given direction, the greater the Rosseland extinction coefficient is. Here, the Glicksman model predicts a significantly higher value of K_R for the BXPS2 foam. Looking at Equation (7), one can see that this is caused by the increase in relative density and the decrease in pore size with respect to BXPS1.

It is remarkable that the ratio of Rosseland extinction coefficients of two directions is, in this case, proportional to the reciprocal of pore sizes, as shown in Equation (12).

$$\frac{K_R^i}{K_R^j} = C\frac{\varphi^j}{\varphi^i}, C = 0.9 \tag{12}$$

This means that changing to a direction with half the pore size will increase the extinction coefficient a proportion of 1.8 times. The coefficient of determination (R^2) was 0.99 in this case.

4.4. Comparison between the three methods

Once the results of all methods have been displayed, it is interesting to discuss whether the methods used were reliable and similar between each other.

In Fig. 7, one can see that, in both materials, the results of all three methods are similar, exhibiting the same tendency $K_{MD} > K_{TD} > K_Z$. In spite of the trend being similar, deviations are found for the Glicksman model in the case of BXPS2, which predicts a much higher extinction coefficient, especially for the lowest pore sizes.

In order to explain this, one must know that the pore walls' thickness decreases linearly with pore size. Those two mechanisms are opposite regarding infrared radiation extinction. Indeed, a maximum of extinction should be expected around 100 μm of pore size as found by *Placido et. Al.* [9] for foams with lower density than the ones used in this work. This phenomenon is not predicted by the Glicksman equation as the assumptions of his equation removes the pore wall thickness parameter. For similar values of f_s and ρ_r, only the pore size makes a difference between both materials in the theoretical equation. Consequently, the Glicksman model predicts a never-ending increase of the radiation extinction when reducing the pore size, which would not be found if lower pore sizes were put to the test, as already found, for nanoporous polymers, by Bernardo et al. [39].

Gathering all the results of the regressions of the ratios extinction coefficients with ratios of pore size (Fig. 8), one can see that there is good agreement between the FTIR and Glicksman methods. Interestingly, a greater dependence of the ratios of K_R with the ratios of pore sizes is found with the subtraction method. Given that none of the used methodologies are purely experimental, as they all include some kind of theoretical approximation, authors believe that the FTIR spectroscopy method is the most reliable one for obtaining the radiative contribution λ_r. This is because, while not being purely experimental, it includes the lowest number of approximations.

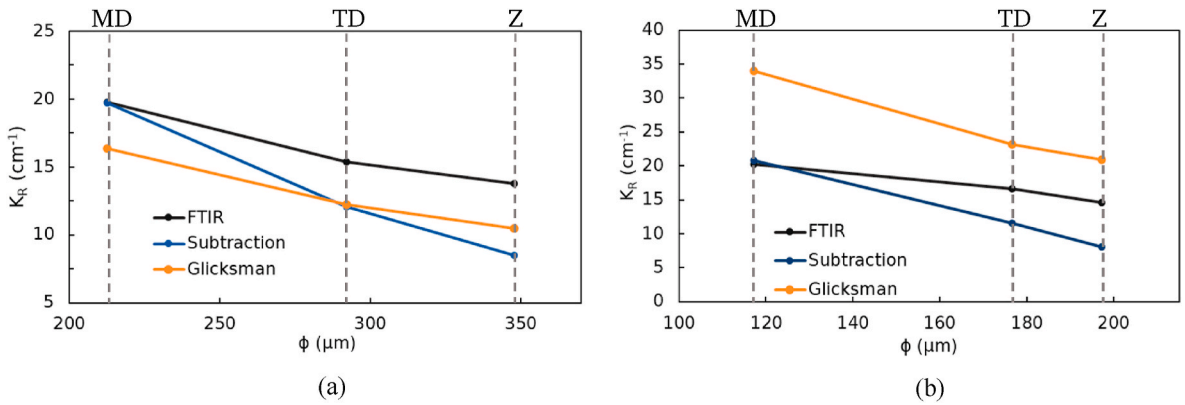

Fig. 7. Summary of the results of K_R obtained by all methods for the samples (a) BXPS1, and (b) BXPS2.

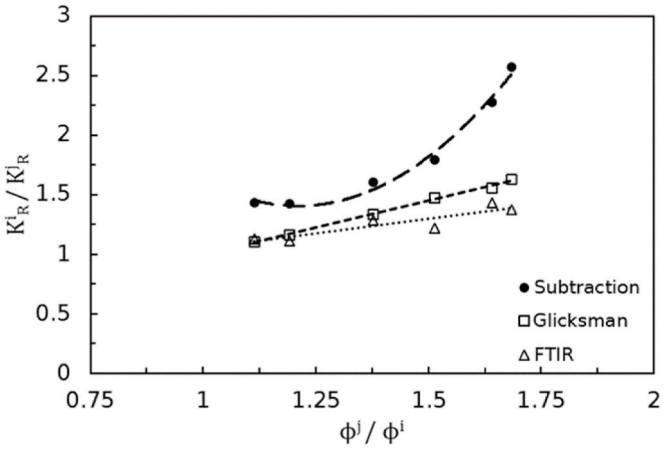

Fig. 8. Summary of the results of the regressions of the ratios of extinction coefficients in two different directions and the reciprocal of their respective pore sizes in all methods for the samples BXPS1 and BXPS2.

4.5. Radiative contribution λ_r to the total thermal conductivity

Once all the results of the Rosseland extinction coefficient are obtained, the radiative contribution can be computed. Fig. 9 shows the values of λ_r for both materials obtained by all the methods previously seen. The overall tendency matches the expected: an increase in the radiative contribution as pore size grows. For the sake of clarity, it must be reminded that this tendency is restricted to the case of microporous polymer foams. In the case of foams with pore size in the nanometric range, the opposite effect would be found, as shown by Bernardo et al. [39].

For both samples, the contributions yielded by each main direction are clearly distinguishable, which proves the existence of different radiative transfer behaviours in each direction. It can be observed that, for both materials, the FTIR and Glicksman methods predict a decrease in the radiative contribution of approximately 1 $mW/(m\,K)$ when reorienting the material from the Z direction to the MD direction. This difference would represent a 20% of the original radiative contribution. On the other hand, the subtraction method predicts a decrease of about 4.5 $mW/(m\,K)$, which would represent a 50% of the original contribution. In any case, this is a remarkable fact, given that these materials are typically applied in the Z direction and used for many years. Using the materials in the direction in which the pore size is smaller (MD direction) can undoubtedly be a significant energy saving.

4.6. All contributions of the heat transfer mechanism

Fig. 10 shows an example of the dependence of the different contributions obtained using the subtraction method with pore size for the samples BXPS1 and BXPS2. Under the hypothesis of the theoretical equations (4) and (5), it seems appropriate to claim that the only mechanism significantly dependent of pore size is the radiative one, i.e., the differences between directions are only due to the different radiation contributions. Comparing between materials, one can see that the contribution of conduction through the gas phase is similar in both materials, while the one in the solid is not, due to the higher relative density of the BXPS2 material. In fact, this contribution is 40% larger in BXPS2 compared to BXPS1, as proved by the ratios of their relative density.

It is also interesting to evaluate the importance of each heat transfer mechanism. It can be observed (see Fig. 11) that the mechanism of

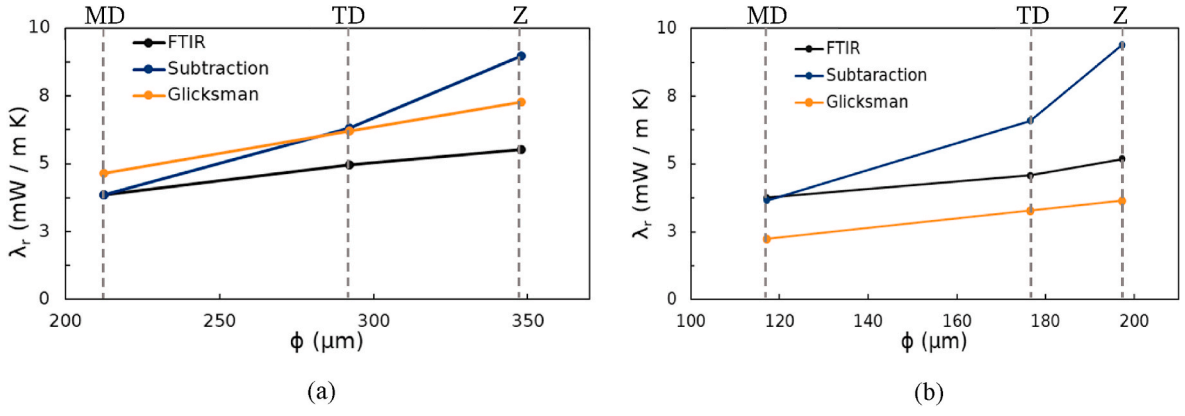

Fig. 9. Summary of the results of λ_r obtained by all methods for the samples (a) BXPS1, and (b) BXPS2.

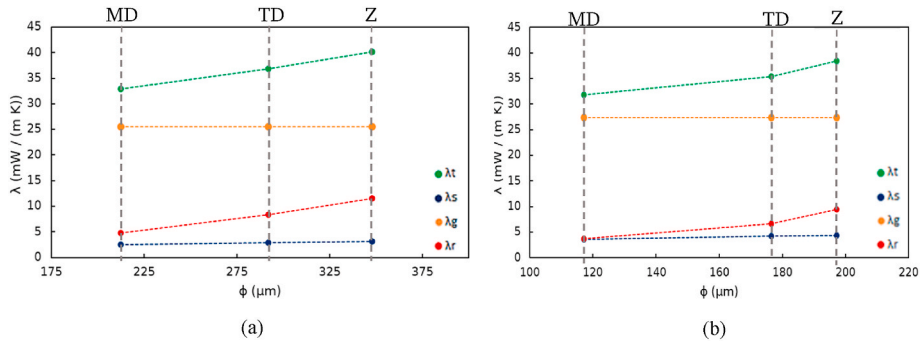

Fig. 10. Dependence of the different contributions and the total conductivity with pore size in the case of (a) BXPS1 and (b) BXPS2 at a mean temperature between the Laser Comp's plates of 20 °C. As λ_s, λ_g and λ_r can be obtained from the equations discussed in the Theoretical Background, the subtraction method was used to obtain these graphs.

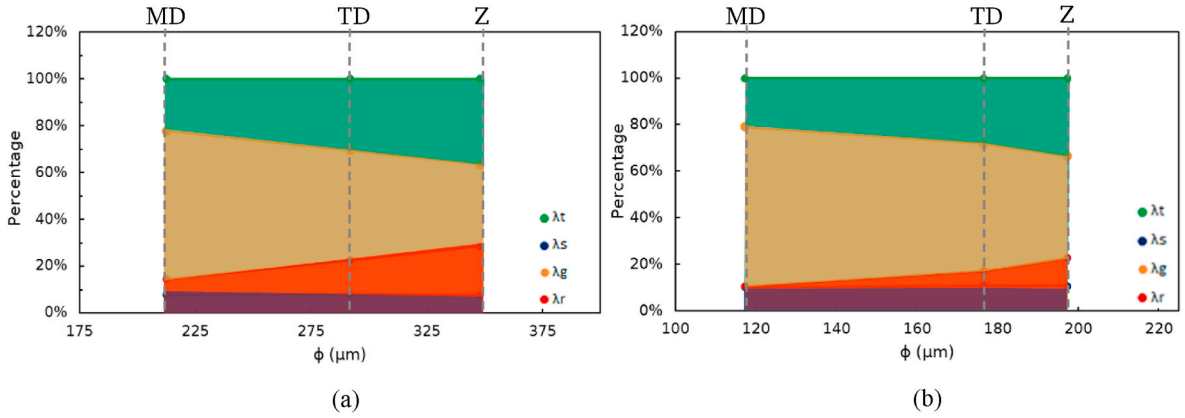

Fig. 11. Dependence of the percentage of all contributions to the total conductivity with pore size in the case of BXPS1 (a) and BXPS2 (b) at a mean temperature between the Laser Comp's plates of 20 °C.

conduction through the gas accounts for about 60 – 80% of the total conductivity in both cases. However, the solid conduction does it only for about 6 – 10%, leaving the radiative transfer mechanism a contribution of around 15 – 30% in BXPS1 and 10 – 20% in BXPS2.

5. Conclusions

Three different methodologies were used to calculate the Rosseland extinction coefficient and, with that, the radiative transfer contribution in anisotropic porous materials with low relative densities. These methodologies are FTIR spectroscopy, derivation from the total conductivity via subtraction of the other contributions, and the theoretical model proposed by Glicksman. First, a characterization of materials was carried out. The selected set of materials was composed of two XPS foams of low density, which were found to have a high anisotropic character, with values of the ratio of anisotropy ranging from about 0.6 in the MD direction to almost 1.4 in the Z direction. Both materials shared the same pore size tendency $\varphi_Z > \varphi_{TD} > \varphi_{MD}$. Regarding the total thermal conductivity, a clear difference between the results in the three directions was found, being the MD direction the one with the lowest values and Z the one with the highest ones.

The results obtained from each methodology revealed significant differences in the contribution of the radiative transfer mechanism to the total thermal conductivity across the principal directions of the porous materials. This study is the first to thoroughly analyze such distinct directional dependencies of radiative transfer in anisotropic polymeric porous materials, addressing directly the thermal insulation performance in practical applications. The findings demonstrate that the anisotropic nature of the materials directly influences their thermal behavior, where larger pore sizes correlate with increased radiative contributions.

The greater the pore size is in one direction, the greater the radiative contribution is in that direction. This is primarily caused by the scattering of infrared radiation in the air-polymer interphases. Particularly, it has been proven that the radiation contribution is larger in Z direction, followed by TD and MD direction. This can affect significantly the performance of polymeric porous materials in their applications as heat insulators, given that, in very anisotropic materials, the values of the total conductivity in each direction may vary considerably due to this behaviour of the radiative transfer. In fact, reorienting the materials from the Z direction to the MD direction may lead to a decrease of up to 10 $mW/(m\,K)$ at high temperatures, in the total conductivity, which represents a difference of about a 20 % with respect to the original. Among these, 5 $mW/(m\,K)$ could be due to the decrease in the radiative contribution. Given that these materials are used for dozens of years, this can end up being a considerable energy saving.

Regarding the methodologies used, FTIR spectroscopy and the subtraction show similar tendencies of the dependence of the radiative contribution with pore size. Also, one can see that there is a good agreement between the results derived from these experimental measurements and the results calculated using the Glicksman's theoretical model.

CRediT authorship contribution statement

Jorge Torre: Writing – review & editing, Writing – original draft, Visualization, Validation, Resources, Methodology, Investigation, Formal analysis, Data curation, Conceptualization. **Victoria Bernardo:**

Resources, Investigation. **Javier Pinto:** Writing – review & editing, Validation, Investigation, Formal analysis, Data curation. **Miguel Ángel Rodríguez-Pérez:** Writing – review & editing, Visualization, Validation, Supervision, Resources, Project administration, Methodology, Investigation, Funding acquisition, Formal analysis, Data curation, Conceptualization.

Declaration of competing interest

The authors declare the following financial interests/personal relationships which may be considered as potential competing interests:

Miguel Angel Rodriguez Perez reports financial support was provided by Spain Ministry of Science and Innovation. Miguel Angel Rodriguez Perez reports financial support was provided by Government of Castile and León. If there are other authors, they declare that they have no known competing financial interests or personal relationships that could have appeared to influence the work reported in this paper.

Data availability

Data will be made available on request.

6. Acknowledgements

This work was supported by Ministerio de Ciencia, Innovación y Universidades (MCIU), Spain (grant numbers: PID2021-127108OB-I00, TED2021-130965B–I00 and PDC2022-133391-I00), Regional Government of Castilla y León and the EU-FEDER program (grant numbers: CLU-2019-04 and C17. I1), which are gratefully acknowledged.

Appendix A. Supplementary data

Supplementary data to this article can be found online at https://doi.org/10.1016/j.polymertesting.2024.108487.

References

[1] European Environment Agency, The European Environment - State and Outlook 2020, 2020, https://doi.org/10.2800/48006.
[2] M. Arduini, J. Manara, C. Vo, Modeling of radiative properties of polystyrene foams containing IR-opacifiers, Cell. Polym. 35 (2016) 49–66, https://doi.org/10.1177/026248931603500201.
[3] C.V. Vo, F. Bunge, J. Duffy, L. Hood, Advances in thermal insulation of extruded polystyrene foams, Cell. Polym. 30 (2011) 137–156, https://doi.org/10.1177/026248931103000303.
[4] C.S. Arroyo, Fabricación De Materiales Celulares Mejorados Basados En Poliolefinas, Relación Procesado-Composición-Estructura-Propiedades, 2013, p. 356, https://doi.org/10.35376/10324/1759.
[5] D. Eaves, Handbook of Polymeric Foams and Foam Technology, Rapra Technology Limited, 2004.
[6] P.G. Collishaw, J.R.G. Evans, An assessment of expressions for the apparent thermal conductivity of cellular materials, J. Mater. Sci. 29 (1994) 2261–2273, https://doi.org/10.1007/BF00363413.
[7] R.A. Campo-Arnáiz, M.A. Rodríguez-Pérez, B. Calvo, J.A. De Saja, Extinction coefficient of polyolefin foams, J. Polym. Sci., Part B: Polym. Phys. 43 (2005) 1608–1617, https://doi.org/10.1002/polb.20435.
[8] A.C.N.C. Hilyard, Low density cellular plastics. https://doi.org/10.1007/978-94-011-1256-7, 1994.
[9] E. Placido, M.C. Arduini-Schuster, J. Kuhn, Thermal properties predictive model for insulating foams, Infrared Phys. Technol. 46 (2005) 219–231, https://doi.org/10.1016/j.infrared.2004.04.001.
[10] D. Doermann, J.F. Sacadura, Heat transfer in open cell foam insulation, J. Heat Tran. 118 (1996) 88–93, https://doi.org/10.1115/1.2824072.
[11] M. Arduini-Schuster, J. Manara, C. Vo, Experimental characterization and theoretical modeling of the infrared-optical properties and the thermal conductivity of foams, Int. J. Therm. Sci. 98 (2015) 156–164, https://doi.org/10.1016/j.ijthermalsci.2015.07.015.
[12] A. Biedermann, C. Kudoke, A. Merten, E. Minogue, U. Rotermund, H.P. Ebert, U. Heinemann, J. Fricke, H. Seifert, Analysis of heat transfer mechanisms in polyurethane rigid foam, J. Cell. Plast. 37 (2001) 467–483, https://doi.org/10.1106/KEMU-LH63-V9H2-KFA3.
[13] N.C. Balaji, M. Mani, B.V.V. Reddy, Discerning heat transfer in building materials, Energy Proc. 54 (2014) 654–668, https://doi.org/10.1016/j.egypro.2014.07.307.
[14] C. Rémi, B. Dominique, Q. Daniel, Radiative properties of expanded polystyrene foams, J. Heat Tran. 131 (2009) 1–10, https://doi.org/10.1115/1.2994764.
[15] A. Kaemmerlen, C. Vo, F. Asllanaj, G. Jeandel, D. Baillis, Radiative properties of extruded polystyrene foams: predictive model and experimental results, J. Quant. Spectrosc. Radiat. Transf. 111 (2010) 865–877, https://doi.org/10.1016/j.jqsrt.2009.11.018.
[16] Marcelo J.S. de Lemos, Andreas Öchsner, Graeme E. Murch, Cellular and Porous Materials Thermal Properties Simulation and Prediction, WILEY-VCH, Weinheim, 2020.
[17] M.A. Schuetz, L.R. Glicksman, A basic study of heat transfer through foam insulation, J. Cell. Plast. 20 (1984) 114–121, https://doi.org/10.1177/0021955X8402000203.
[18] R.J.J. Williams, C.M. Aldao, Thermal conductivity of plastic foams, Polym. Eng. Sci. 23 (1983) 293–298, https://doi.org/10.1002/pen.760230602.
[19] J. Kuhn, H.P. Ebert, M.C. Arduini-Schuster, D. Büttner, J. Fricke, Thermal transport in polystyrene and polyurethane foam insulations, Int. J. Heat Mass Tran. 35 (1992) 1795–1801, https://doi.org/10.1016/0017-9310(92)90150-Q.
[20] R. Caps, U. Heinemann, J. Fricke, K. Keller, Thermal conductivity of polyimide foams, Int. J. Heat Mass Tran. 40 (1997) 269–280, https://doi.org/10.1016/0017-9310(96)00134-2.
[21] C. jen Tseng, K. te Kuo, Thermal radiative properties of phenolic foam insulation, J. Quant. Spectrosc. Radiat. Transf. 72 (2002) 349–359, https://doi.org/10.1016/S0022-4073(01)00129-7.
[22] J.E. Arconada, Polyolefin based cellular materials. Development of New Production Routes and Optimization of Barrier and Mechanical Properties by the Addition of Nanoclays, 2015, https://doi.org/10.35376/10324/16561.
[23] P. G., B. Vergnes, Polymer Extrusion, Wiley, Hoboken (USA), 2014.
[24] C.V. Vo, A.N. Paquet, An evaluation of the thermal conductivity of extruded polystyrene foam blown with HFC-134a or HCFC-142b, J. Cell. Plast. 40 (2004) 205–228, https://doi.org/10.1177/0021955X04043719.
[25] F.M.E. Duddeck, S.D. Poisson, Heat conduction. https://doi.org/10.4324/9780203477380-8, 2002.
[26] R.J. Schmidt, Advanced mechanics of materials (1953), https://doi.org/10.1016/0016-0032(53)90801-1.
[27] V. Bernardo, J. Martin-de Leon, M.A. Rodriguez-Perez, Anisotropy in nanocellular polymers promoted by the addition of needle-like sepiolites, Polym. Int. 68 (2019) 1204–1214, https://doi.org/10.1002/pi.5813.
[28] J.P. Holman, Heat Transfer, tenth ed., McGraw-Hill, New York, 2010.
[29] B. Notario, J. Pinto, E. Solorzano, J.A. De Saja, M. Dumon, M.A. Rodríguez-Pérez, Experimental validation of the Knudsen effect in nanocellular polymeric foams, Polymer 56 (2015) 57–67, https://doi.org/10.1016/j.polymer.2014.10.006.
[30] S.S. Shrestha, J. Tiwari, A. Rai, D.E. Hun, D. Howard, A.O. Desjarlais, M. Francoeur, T. Feng, Solid and gas thermal conductivity models improvement and validation in various porous insulation materials, Int. J. Therm. Sci. 187 (2023) 108164, https://doi.org/10.1016/j.ijthermalsci.2023.108164.
[31] CellMat Technologies – Software and methodology for the characterization of cellular structures, (n.d.). http://www.cellmattechnologies.com/en/software-and-methodology-for-the-characterization-of-cellular-structures/(accessed March 13, 2023).
[32] P. Cimavilla-Román, S. Pérez-Tamarit, S. Barroso-Solares, J. Pinto, M.Á. Rodríguez-Pérez, Sub-pixel tomographic methods for characterizing the solid architecture of foams, Microsc. Microanal. 28 (2022) 689–700, https://doi.org/10.1017/S1431927622000447.
[33] M.D. Abràmoff, P.J. Magalhães, S.J. Ram, Image processing with imageJ, Biophot. Int. 11 (2004) 36–41, https://doi.org/10.1201/9781420005615.ax4.
[34] Peak analysis with Peakfit, (n.d.). https://systatsoftware.com/peakfit/(accessed March 15, 2023).
[35] M. Tasumi, Introduction to Experimental Infrared Spectroscopy, (n.d.) 404.
[36] J. Meseguer, I. Pérez-Grande, A. Sanz-Andrés, Thermal Radiation Heat Transfer, 2012, https://doi.org/10.1533/9780857096081.73.
[37] J. Brier, lia dwi jayanti, Principios de transferencia de calor, seventh ed., 2020. http://journal.um-surabaya.ac.id/index.php/JKM/article/view/2203.
[38] Standard Test Method for Steady-State Thermal Transmission Properties by Means of the Heat Flow Meter Apparatus., (n.d.). https://www.astm.org/c0518-21.html (accessed May 29, 2022).
[39] V. Bernardo, J. Martin-de Leon, J. Pinto, U. Schade, M.A. Rodriguez-Perez, On the interaction of infrared radiation and nanocellular polymers: first experimental determination of the extinction coefficient, Colloids Surfaces A Physicochem. Eng. Asp. 600 (2020), https://doi.org/10.1016/j.colsurfa.2020.124937.